International Journal of Lightweight Materials and Manufacture 8 (2025) 301–309

Contents lists available at ScienceDirect

International Journal of Lightweight Materials and Manufacture

journal homepage: www.keaipublishing.com/ijlmm

Original Article

Enhancing the performance of laser powder bed fusion through hybridization with bending

Valentino A.M. Cristino [a], Rui FV. Sampaio [b], João P.M. Pragana [b], Ivo M.F. Bragança [c], Carlos M.A. Silva [b], Paulo A.F. Martins [b, *]

[a] Department of Electromechanical Engineering, University of Macau, Avenida da Universidade, Taipa, Macao, China
[b] IDMEC, Instituto Superior Tecnico, Universidade de Lisboa Av. Rovisco Pais, 1049-001 Lisboa, Portugal
[c] CIMOSM, Instituto Superior de Engenharia de Lisboa, Instituto Politécnico de Lisboa, Portugal

ARTICLE INFO

Article history:
Received 29 November 2024
Received in revised form
9 December 2024
Accepted 10 December 2024
Available online 14 December 2024

Keywords:
Hybrid additive manufacturing
Laser powder bed fusion
Bending
Formability
Finite element method
Experimentation

ABSTRACT

This paper is focused on the hybridization of metal additive manufacturing with bending to shape thin-walled deposited materials into fully three-dimensional custom parts with specific angles. The presentation covers material deposition by laser powder bed fusion, material and formability characterization using tension and three-point bending tests, and proof-of-concept validation through bending a flat, cross-shaped, deposited plate into a slender three-dimensional double U-shaped part. The use of digital image correlation and finite element analysis supports the presentation as well as the design and creation of the part. Results underscore the significance of hybridizing metal additive manufacturing with bending due to the gains obtained in material usage and fabrication time of 87.9 % and 85.7 %, respectively. The overall methodology integrating material deposition, formability analysis, and combined experimental and finite element simulation of bending proves effective for designing hybrid metal additive-manufactured parts, providing a comprehensive framework for future research and development in this area.

1. Introduction

Laser powder bed fusion (LPBF) is a metal additive manufacturing (MAM) process that utilizes thermal energy from a laser beam to melt and consolidate powder into complex parts [1]. The laser beam moves according to a predefined two-dimensional scanning path to create the parts layer upon layer in a controlled atmosphere of argon or nitrogen, depending on whether the metal is reactive.

Although LPBF offers significant benefits, such as the ability to create customized parts with complex geometries, intricate details, and reduced material waste across various metals, several challenges still hinder its adoption as an alternative manufacturing process. Besides the high cost of the equipment, challenges are fundamentally related to longer production times compared to traditional manufacturing processes, the size of the parts that can be created in a single build, and the need for significant post-processing operations to remove support structures, obtain the required tolerances and finishing, and compensate for the distortions arising from thermal residual stresses induced by the heating and cooling cycles during material deposition.

Fig. 1a shows a schematic representation of a metal additive manufacturing route to fabricate a slender, three-dimensional conceptual S-shaped part, from material deposition to the post-processing operations needed to obtain the final part.

In recent years, various manufacturing routes built upon concurrent or sequential integrations of MAM with traditional manufacturing processes have been proposed to address the above-mentioned difficulties associated with the existing additive manufacturing processes [2]. Metal cutting, for example, has been extensively used to improve both geometric precision and surface quality of the as-built parts during post-processing [3]. However,

* Corresponding author.
E-mail addresses: vcristino@um.edu.mo (V.A.M. Cristino), rui.f.sampaio@tecnico.ulisboa.pt (R.FV. Sampaio), joao.pragana@tecnico.ulisboa.pt (J.P.M. Pragana), ibraganca@dem.isel.ipl.pt (I.M.F. Bragança), carlos.alves.silva@tecnico.ulisboa.pt (C.M.A. Silva), pmartins@tecnico.ulisboa.pt (P.A.F. Martins).

Peer review under the responsibility of Editorial Board of International Journal of Lightweight Materials and Manufacture.

https://doi.org/10.1016/j.ijlmm.2024.12.003
2588-8404/

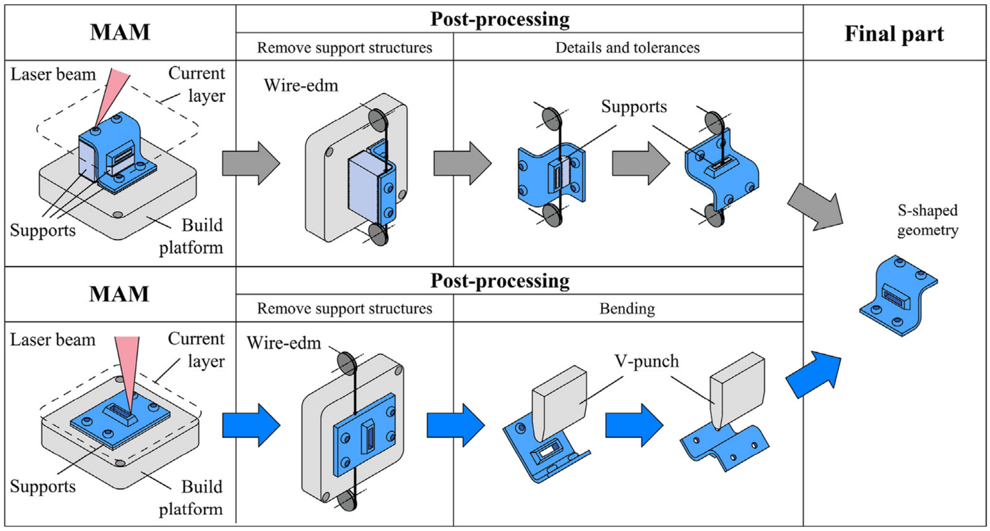

Fig. 1. Schematic representation of two manufacturing routes to fabricate a three-dimensional, slender conceptual S-shaped part, using:
(a) Metal additive manufacturing (MAM) consisting of laser powder bed fusion (LPBF).
(b) Hybrid metal additive manufacturing resulting from the combination of laser powder bed fusion (LPBF) with bending.

integrating MAM with metal cutting during material deposition [4] is time-consuming, especially for large parts, resulting in significant additional production times.

Integrating MAM with metal forming is a promising solution to expand its applicability from unitary to batch production. Several researchers have recently explored this trend, highlighting the potential of MAM to produce preforms and near-net-shape parts in small to medium batch sizes for subsequent processing with traditional sheet [5], bulk [6], and sheet-bulk [7] forming operations.

Fig. 1b shows a schematic representation of an alternative hybrid additive manufacturing route combining metal additive manufacturing with bending to fabricate the same slender, three-dimensional conceptual S-shaped part faster and with fewer post-processing operations to remove support structures and ensure the required dimensions.

Despite the importance of the topic, the number of publications on the hybridization of MAM, namely LPBF, with bending has been reduced and consists of two main types. The first publication type focuses on bending commercial rolled sheets with additively manufactured elements deposited away from Ref. [8] or on top of [9] the plastically deforming regions before or after bending. In the case of elements deposited on top of the plastically deforming regions of commercially rolled sheets, studies are primarily focused on the bonding stresses between the elements and sheets, considering the stress states resulting from the bending process [9], on the distortion of the parts resulting from different material deposition strategies and on the resulting microstructures and mechanical properties derived from different heat treatments [10]. The results gathered from these studies are encouraging and confirm the positive impact of homogeneous microstructures and decreased hardnesses on the hybridization of LPBF with bending.

The second publication type focuses on the bending of sheets deposited by LPBF. One of the earlier works in the field [11] investigated the material flow behavior of nickel-based superalloy (Hastelloy X) deposited sheets, using a variety of tension, torsion, compression, and bulge tests. Results show that the as-built sheets are highly anisotropic and require heat treatment to recrystallize their grain microstructure and approximate their behavior to that of commercial hot-rolled sheets used in traditional manufacturing processes.

The potential of hybridizing LPBF with bending was recently further explored with research on additively deposited AISI 316L stainless steel sandwich sheets with various core structures (similar to sandwich sheets) [12]. Results conclude that hybridization opens the opportunity to increase the overall efficiency of the manufacturing route from 40 % up to 680 % compared to pure additive manufacturing by LPBF due to less material waste and much better time and energy efficiencies.

Despite the potential benefits of hybridizing LPBF with bending claimed in the above publications, studies continue to highlight the persistent difficulties related to the formability problems of the deposited materials [13]. Deposited materials often exhibit irregular columnar microstructures caused by dendritic growth due to the heating-cooling cycles taking place during layer-by-layer construction, and for this reason, they generally have lower formability than their corresponding commercial (casted or wrought) counterparts. Heat treatments such as annealing are commonly used to address or mitigate this problem.

However, because there are situations where the as-built metal, without any post-processing, exhibits sufficient ductility to withstand high levels of plastic deformation without cracking, this leads to the conclusion that the decision to use heat treatments after metal deposition is mainly dependent on the overall plastic deformation requirements to shape the deposited metal into its final form. Consequently, the hybridization of LPBF with bending underscores the necessity for further research into the formability limits of deposited materials when subjected to significant levels of plastic deformation.

Under these circumstances, this paper focuses on the formability of sheets deposited by LPBF. It employs tension and three-point bending tests to perform mechanical and formability characterization of the material in both as-built and heat-treated conditions, with the in-plane strains during tests being measured through digital image correlation (DIC). The fracture forming limit, which defines the maximum plastic deformation during bending in principal strain space, is then used to design and fabricate a three-dimensional double U-shaped part. This part serves as an example to highlight the effectiveness of the overall methodology and hybridization of LBPF with bending.

2. Materials and methods

2.1. Materials and deposition

The work was carried out in gas-atomized AlSi10Mg aluminum alloy powder (hereafter referred to as 'aluminum alloy powder' or simply 'powder'), whose chemical composition is presented in Table 1. Scanning electron microscopy (SEM) of the aluminum alloy powder in a Hitachi S–3400 N, Type I model provided an average diameter of 26–63 μm (Fig. 2).

Three different specimens, aligned with the geometries required for the investigation, were constructed by LPBF in an SLM 280HL 2.0 system equipped with a 400W laser. The building process was performed under a controlled atmosphere of nitrogen to ensure an oxygen content below 0.1 %, and the build platform was maintained at a temperature of 150 °C throughout the construction of the specimens. Table 2 provides a comprehensive summary of the main parameters used in the deposition of the specimens.

The laser scanned and fused the powder layers at a speed of 1335 mm/s with a spot size of 80 μm. The specimens were built horizontally to minimize the use of support structures and diminish the thermal gradients between the top and bottom layers. Deposition consisted of a strip-like strategy with a hatch spacing of 0.15 mm and a strip length of 10 mm, which was rotated 67° after completing each layer to avoid repetition (refer to the bottom specimen picture in Table 2).

After finishing material deposition, the specimens were removed from the substrate by wire electrical discharge machining (wire-EDM) using a DK350 machine of Datie Numerical Control Machinery with a wire diameter of 0.18 mm and finished by milling to calibrate the final thickness. Some specimens were heat treated by annealing at 320 °C for 3 h, followed by cooling in the furnace, while others were left in the as-built condition.

2.2. Mechanical and formability tests

The specimens constructed for the tension and three-point bend tests were machined (milled) to a final thickness $t = 3$ mm to provide perfect parallel surfaces and final geometries in accordance with the ASTM E8/E8M – 16 [14] and ASTM E290–14 [15] standards, respectively. Fig. 3 provides a scheme of the tension and three-point bend tests with an indication of the geometry of the corresponding specimens.

Table 1
Chemical composition of the AlSi10Mg aluminum alloy powder used in LPBF.

Element	Al	Si	Mg	Fe	Zn	Ti	Cu	Mn
wt%	Balance	10	0.4	0.13	0.01	0.01	0.01	0.01

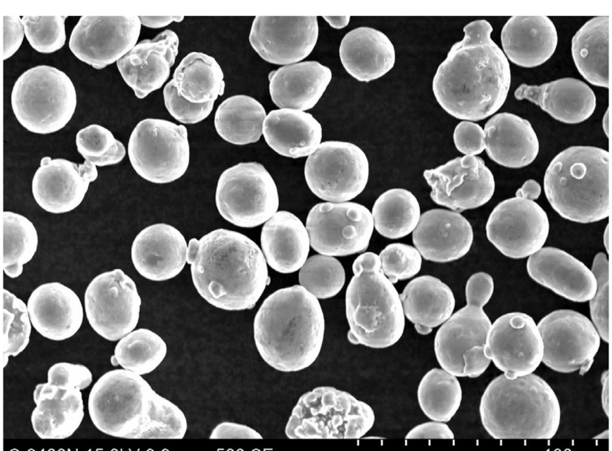

Fig. 2. Scanning electron microscopy of the AlSi10Mg aluminum alloy powder used in LPBF.

The tension tests were carried out in an INSTRON 5900 universal testing machine, whereas the three-point bend tests were performed in an INSTRON SATEC 1200 kN with the assistance of a multidirectional toolset [16]. The tool set was used to convert the vertical stroke into a horizontal movement using a cam slide unit consisting of a cylindrical punch moving against two cylindrical support fixtures placed at a distance apart and holding the specimens in place. Both tests allowed the evolution of the in-plane strains to be obtained over time $\varepsilon_1(t)$, $\varepsilon_2(t)$ using a commercial digital image correlation (DIC) system from Dantec Dynamics (model Q-400 3D).

The system featured two 6-megapixel resolution cameras equipped with 50.2 mm focal length lenses and f/8 aperture (Fig. 3a and b), and a spotlight illuminated the region of interest during testing. Images were captured by the cameras at a shutter frequency of 20 Hz and analyzed with the INSTRA 4D software from Dantec Dynamics.

Combining the evolutions of in-plane strains over time $\varepsilon_1(t)$, $\varepsilon_2(t)$ by removing the time dependency allowed the strain loading paths in principal strain space $\varepsilon_1 = f(\varepsilon_2)$ to be obtained up to fracture.

2.3. Hybrid additive manufacturing test

The hybrid additive manufacturing test involved fabricating three-dimensional double U-shaped parts from flat, cross-shaped, specimens through a sequence that combined material deposition using LPBF and plastic deformation by bending.

Unlike the traditional tension and three-point bend tests, the specimens used in this test were directly removed from the substrate by wire-EDM and subjected to heat treatment by annealing. The absence of finishing by milling in one surface side gave the specimens a surface with the as-built rough texture, a feature that significantly reduced the number of post-processing operations, enhancing the practicality and efficiency of the hybridization of LPBF with bending. Fig. 4a and b provide the geometry of the specimens and final three-dimensional double U-shaped parts, along with details of the punch and die tool set used in the bending operations.

A three-dimensional double U-shaped part exclusively made by LPBF using a conventional additive manufacturing route was used for reference purposes, namely, to compare material usage and fabrication time of the conventional and hybrid additive manufacturing routes.

2.4. Numerical simulation

Bending of the flat cross-shaped specimens was carried out using an in-house finite element computer program [17] built upon a modified weak form of Markov's rate of energy variational statement to include contact and sliding with friction between the specimens and the punches and die of the tool set,

$$\int_V \sigma'_{ij}\delta D_{ij}dV + \int_V \sigma_m \delta D_v dV - \int_{S_t} t_i \delta u_i dS + \int_{S_f}\left(\int_0^{|u_r|} \tau_f \delta u_r\right) dS = 0 \tag{1}$$

The expression above adopts a control volume V approach incorporating a sort of 'updated Eulerian approach' with velocities u_i as the primary unknowns [18]. The first term of the expression

Table 2
Main parameters and deposition strategy utilized in the fabrication of the three different specimen geometries using LPBF.

Laser power	370 W
Spot size	80 μm
Scanning speed	1335 mm/s
Layer thickness	30 μm
Hatch spacing	0.15 mm
Scan pattern	Stripe
Strip length	10 mm
Scan rotation	67°

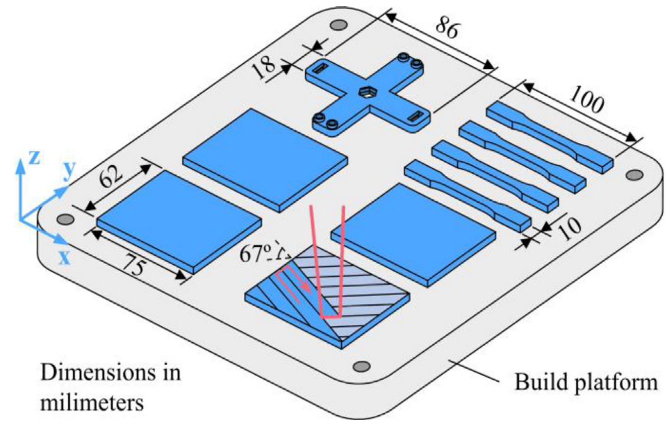

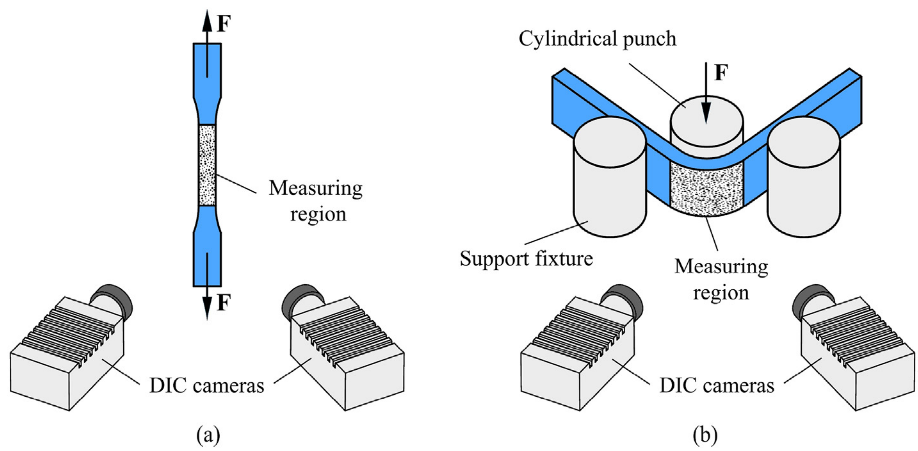

Fig. 3. Schematic representation of the (a) tension and (b) three-point bend tests, along with the geometry of the specimens and details of the setups utilized by the DIC system.

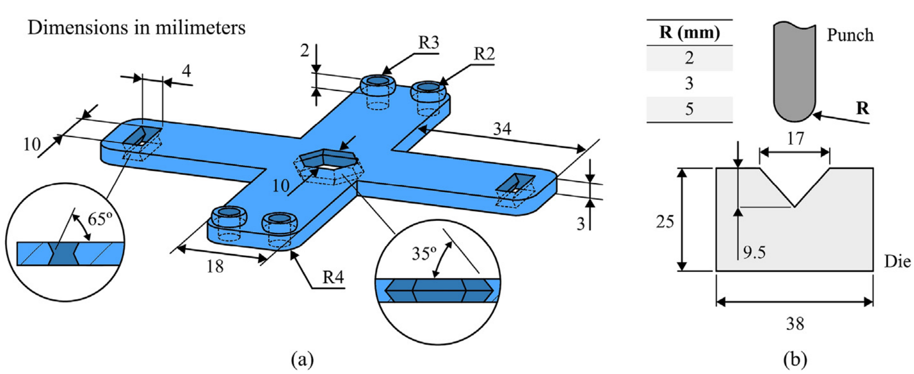

Fig. 4. (a) Geometry of the flat cross-shaped specimens and final three-dimensional double U-shaped parts. (b) Schematic representation of the punch and die tool set used in the bending operations.

involves the deviatoric Cauchy stress σ'_{ij} and the rate of deformation D_{ij}, representing viscous effects. The second term makes use of the hydrostatic stress σ_m and the volumetric rate of deformation D_v, analogous to hydrostatic effects on a viscous fluid. The incompressibility condition of the velocity field $D_v = 0$ is relaxed using a penalty function K, where $\sigma_m = (K/2)D_v$. The third and fourth terms in (1) refer to the tractions t_i applied on the boundary S_t of the control volume, and to the friction shear stress τ_f and the relative sliding velocity u_r acting on the contact interfaces S_f between the specimens and the punches and dies.

Friction was modelled using the law of constant friction, expressed as $\tau_f = mk$, where k represents the shear flow stress and m denotes the friction factor. The latter was taken as 0.1 after checking the value that provided the best match between the experimental and predicted finite element force-displacement evolutions.

The material was assumed to be isotropic, following the Levy-Mises constitutive equations, with a flow stress that will be provided later, along with other information, in the section of 'Results and Discussion'.

The specimens were discretized with meshes consisting of approximately 7500 hexahedral elements. Similarly, the different punches and die were discretized with contact-friction spatial triangles. Fig. 5 presents a typical finite element model used to simulate one bending operation and making use of symmetry conditions along the *xz* and *yz* planes.

The average computation time for an Intel(R) Core(TM) i7-6950X with a CPU of 3.00 GHz was around 45 min.

3. Results and Discussion

3.1. Heat treatment

The microstructure of both as-built and annealed aluminum alloy specimens deposited by LPBF was examined with an optical microscope DMI3000 M from Leica. The specimens were initially cut using wire-EDM, and their surfaces were subsequently ground using progressively finer silicon carbide (SiC) paper, starting with 320 grit and moving up to 2000 grit. The final polishing was done with velvet cloth and 0.5 μm diamond paste. Before observation, the samples were etched in a 30 % sodium hydroxide (NaOH) solution for approximately 30 s. After etching, they were cleaned with a 3 % nitric acid (HNO3) solution, rinsed with water, and dried.

Fig. 6a depicts the microstructure of the as-built specimens deposited by LPBF. Observation allows the identification of individual melt pools with borders consisting of fine dendrite structures, which is the result of rapid solidification rates and the reheating effects produced by the overlaying passes during layer-by-layer material deposition by LPBF [19].

In contrast, the microstructure of the specimens after annealing at 320 °C for 3 h, shown in Fig. 6b, reveal that the boundaries of melt pools disappeared completely. These microstructures will later be used to justify the influence of annealing on the mechanical properties and formability behavior of the deposited aluminum alloy.

3.2. Mechanical and formability characterization

Fig. 7a presents the flow curves (true stress vs. true strain curves) of the as-built and annealed aluminum alloy deposited by LPBF obtained from tension tests.

As seen, the flow curve of the as-built aluminum alloy shows higher strength and lower elongation at fracture than that of the annealed aluminum alloy. These differences are attributed to the dendritic-based microstructure of the as-built aluminum alloy, and the reduction in ductility is also observed in the evolution of the corresponding strain loading path in principal strain space obtained by DIC. In fact, as shown in Fig. 7b, the as-built aluminum alloy specimens present strain values at fracture much smaller than those of the annealed aluminum alloy specimens (refer to the X-markers of the tension test in the second quadrant).

Other mechanical properties listed in Table 3 also show differences between the aluminum alloy deposited by LPBF in the as-built and annealed conditions.

Fig. 7b also shows the strain loading path in principal strain space $\varepsilon_1 = f(\varepsilon_2)$ up to the end of the three-point bend test obtained from DIC for test specimens made of aluminum alloy powder deposited by LPBF and subsequently annealed. Unlike the tension tests, no cracks were observed in the material. This suggests that the fracture forming limit of the material, represented by a black line, must be established by drawing a line with a slope of '-1' (as specified in Ref. [20]) through the average values of the in-plane strain at fracture, which were obtained solely from the tension tests.

Three-point bend tests were not performed with as-built specimens made from the aluminum alloy powder deposited by LPBF due to the reduced ductility observed in the tension tests.

3.3. Hybrid additively manufactured double U-shaped part

The punch and die design was carried out through finite element and formability analysis, using data retrieved from the mechanical and formability material characterization tests. The aim was to select two different cylindrical punch radii capable of ensuring successful and unsuccessful forming due to the absence or occurrence of cracks in order to validate the overall methodology to design and fabricate hybrid additively manufactured parts by a combination of material deposition by LPBF and bending.

Fig. 8 shows the finite element computed distribution of accumulated damage D^{Mc} using the McClintock ductile fracture criterion [21] for the two different punch radii at the end of the first bending operation required to fabricate a three-dimensional double U-shaped part of a flat, cross-shaped, deposited plate.

The choice of McClintock's criterion,

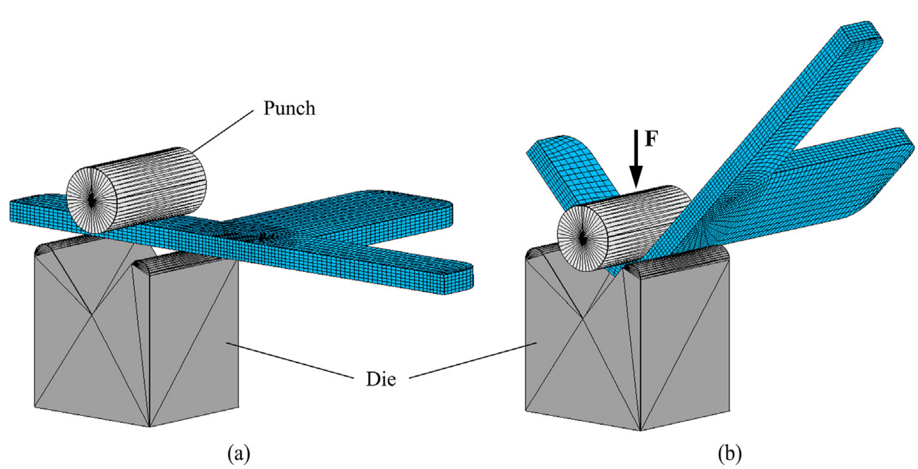

Fig. 5. Finite element modelling (half-section) of a flat cross-shaped specimen at the (a) beginning and (b) end of bending.

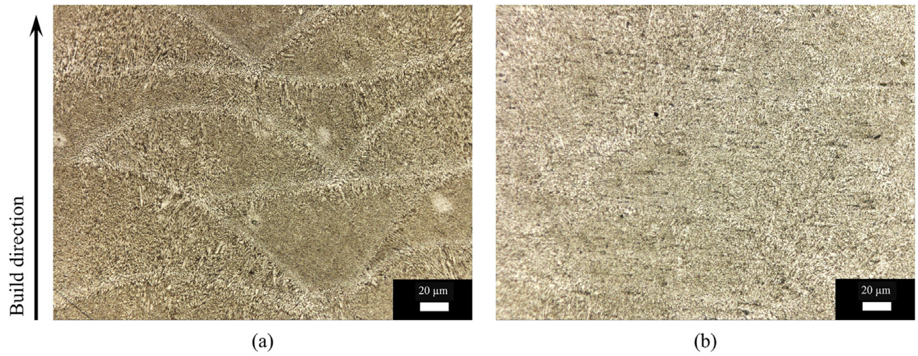

Fig. 6. Microstructure observations of metallurgical samples extracted from aluminum alloy specimens deposited by LPBF (a) not subjected to annealing and (b) subjected to annealing.

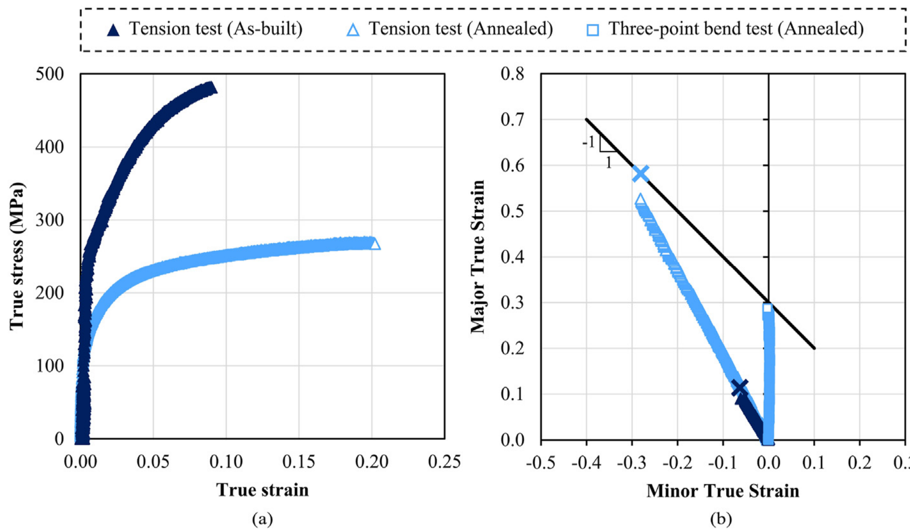

Fig. 7. Mechanical and formability characterization of the aluminum alloy deposited by LPBF.
(a) Flow curves of the material in the as-build and annealed conditions, obtained from tension tests
(b) Strain loading paths obtained by DIC during tension and three-point bend tests.

Table 3
Summary of the mechanical properties of the aluminum alloy deposited by LPBF in the as-built and annealed conditions.

	Yield Strength σ_Y (MPa)	Ultimate Tensile Strength σ_{UTS} (MPa)	Elongation at Break A (%)
As-built	262.9	440.9	9.4
Annealed	133.5	227.6	26.9

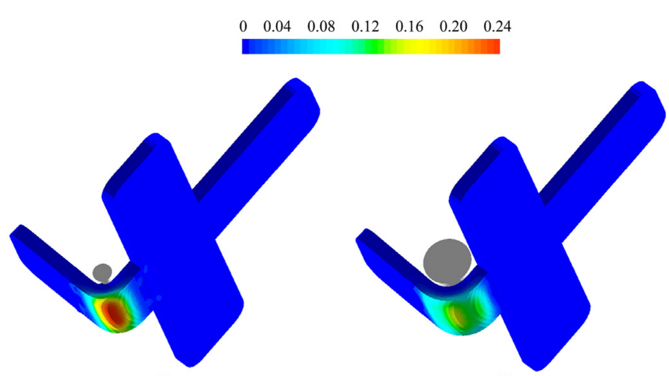

Fig. 8. Finite element computed distribution of damage according to the McClintock ductile fracture criterion at the end of the first bending operation and using punches with (a) 2 mm and (b) 5 mm radius.

$$D^{Mc} = \int_0^{\bar{\varepsilon}} \eta d\bar{\varepsilon} \tag{2}$$

where $\bar{\varepsilon}$ is the effective strain, and $\eta = \sigma_m/\bar{\sigma}$ is the stress triaxiality, accounted for crack opening by tension (mode I of fracture mechanics) being the likely mode of failure in the outer radius of the parts subjected to tensile stresses [20].

As shown in Fig. 8, the part subjected to bending with a punch of 2 mm radius accumulates more damage, giving rise to a strain loading path that goes beyond the fracture forming limit obtained from the material formability characterization performed in Section 3.2. This result aligns with the previously established critical damage threshold at fracture for the deposited material, which is 0.21, as determined by the authors.

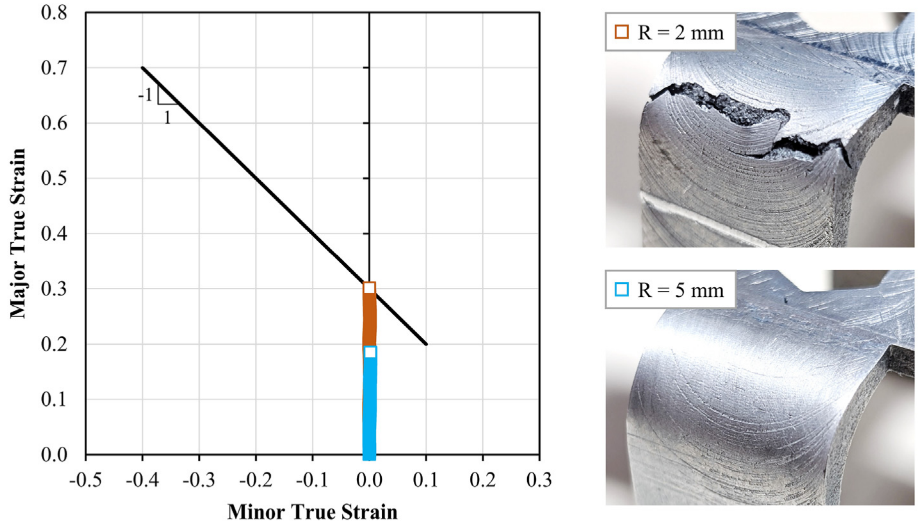

Fig. 9. Finite element computed strain loading paths experienced by the outer radius during bending of flat, cross-shaped, deposited plates into a three-dimensional double U-shaped part. Photographs show details of the outer radii $R = 2\ mm$ (with a crack) and $R = 5\ mm$ (without a crack) for the bent arms of the corresponding double U-shaped parts.

The consequence of exceeding this critical damage value is illustrated in Fig. 9, where a photograph of the fractured region of the hybrid additively manufactured three-dimensional double U-shaped part discloses cracks perpendicular to the acting tension stresses. This emphasizes the importance of knowing the critical damage values and fracture forming limits to improve the selection and design of hybrid manufacturing processes that combine additive manufacturing with bending.

In contrast, the other part subjected to bending with a punch of 5 mm radius accumulates less damage, giving rise to a strain

Table 4
Summary of the material usage and fabrication time of the conventional and hybrid additive manufacturing routes to fabricate the three-dimensional double U-shaped part of AlSi10Mg aluminum alloy.

Manufacturing route	Build volume	Material used	Operational time	Final part
Conventional AM	541.2 cm^3	1.445 kg	8h58 m	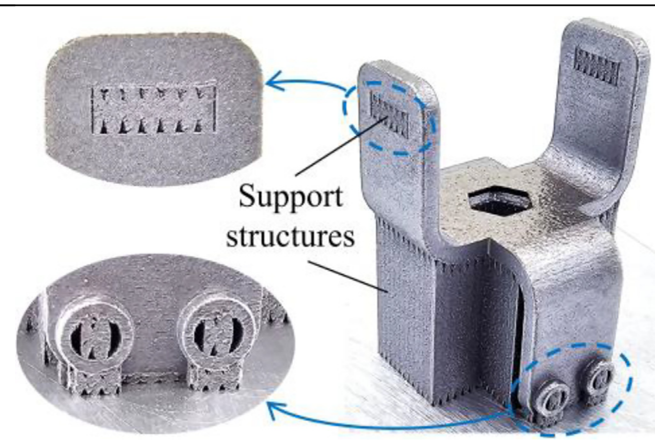
Hybrid AM	65.1 cm^3	0.174 kg	1h17 m	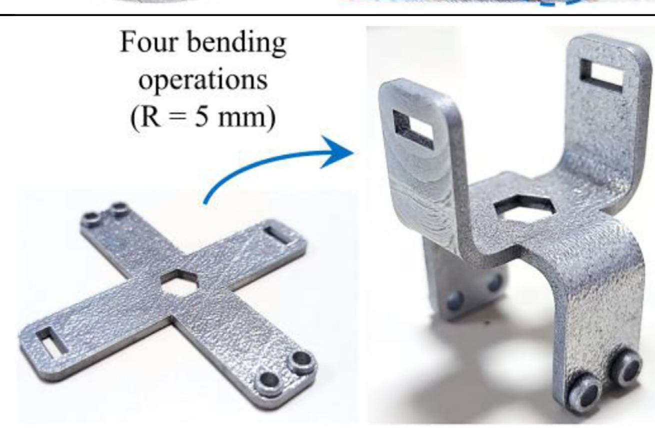

loading path that ends below the fracture forming limit, in close agreement with the fabrication of a sound hybrid additively manufactured double U-shaped part.

To conclude, Table 4 shows a comparison between material usage and fabrication time in the construction of the three-dimensional double U-shaped parts using a conventional additive manufacturing route solely based on LPBF and the hybrid additive manufacturing route resulting from the combination of LBPF and bending.

The build volume consists of the predicted part volume (obtained from CAD files) and the support structures used to reduce inaccuracies in the first layers of powder spreading, support material overhangs, and minimize warping. The values were defined in the system software before the layer-by-layer construction by LPBF began.

The amount of material used corresponds to the powder feedstock that is effectively melted and consolidated onto the semi-finished deposited part, along with the necessary support structures. Like in the former case, the LPBF system software also predicted these values, which were later verified through weight measurements on a commercial scale.

Finally, the operational time refers only to that spent during metal deposition by LPBF. For this reason, it consists of the LPBF system's operational time upon which the laser scanning strategy, interlayer cooling and recoating were employed.

As concluded from Table 4, the hybrid additive manufacturing route leads to 87.9 % material savings and a significant reduction in the overall built time (approximately 85.7 %) because the bending operations are carried out almost instantaneously. These results suggest lower production costs and strongly support the validity of the newly proposed hybrid additive manufacturing route.

4. Conclusions

The main conclusions that can be drawn from this investigation on the hybridization of laser powder bed fusion with bending are the following:

- Hybrid manufacturing routes based on the combination of LPBF and bending provide significant reductions in material consumption and construction time,
- Bending of the as-built LPBF preforms requires them to be subjected to heat treatment to eliminate the fine type dendritic-based microstructures resulting from the overlaying passes during layer-by-layer material deposition and obtain small-sized equiaxed grains-based structures with better ductility,
- The fracture forming limit line of the LPBF preforms subjected to heat treatment is located significantly above the in-plane fracture strain values obtained for the as-built material in principal strain space, indicating that the material's ductility has been significantly improved,
- Finite element predictions of damage using the McClintock ductile fracture criterion show good agreement with both fracture forming limits obtained from tension and three-point bending tests and experimental bending operations carried out with two different punch radii.
- The results underscore the importance of hybrid additive manufacturing built upon a combination of LPBF and bending, and the role played by finite elements in providing a solid ground for designing the overall manufacturing routes.

CRediT authorship contribution statement

Valentino A.M. Cristino: Writing – review & editing, Validation, Resources, Project administration, Methodology, Investigation, Funding acquisition, Formal analysis, Data curation, Conceptualization. **Rui FV. Sampaio:** Writing – review & editing, Validation, Resources, Methodology, Investigation, Formal analysis, Data curation. **João P.M. Pragana:** Writing – review & editing, Writing – original draft, Visualization, Validation, Software, Resources, Methodology, Investigation, Formal analysis, Data curation, Conceptualization. **Ivo M.F. Bragança:** Writing – review & editing, Validation, Supervision, Resources, Methodology, Investigation, Formal analysis, Data curation, Conceptualization. **Carlos M.A. Silva:** Writing – review & editing, Validation, Supervision, Resources, Project administration, Methodology, Investigation, Funding acquisition, Formal analysis, Data curation, Conceptualization. **Paulo A.F. Martins:** Writing – original draft, Validation, Supervision, Software, Project administration, Methodology, Investigation, Funding acquisition, Formal analysis.

Declaration of competing interest

The authors declare that there is no conflicts of interest.

Acknowledgments

The authors would like to acknowledge the support provided by Fundação para a Ciência e a Tecnologia of Portugal (FCT) and IDMEC for its financial support via the project LAETA Base Funding (DOI: 10.54499/UIDB/50022/2020). Rui F.V. Sampaio would also like to acknowledge the support under the PhD Studentship 2022.12351.BD. Valentino Cristino would like to acknowledge the support provided by the Science and Technology Development Fund of Macao (grant no. 0087/2021/A2).

References

[1] S. Chowdhury, N. Yadaiah, C. Prakash, S. Ramakrishna, S. Dixit, L.R. Gupta, D. Buddhi, Laser powder bed fusion: a state-of-the-art review of the technology, materials, properties and defects, and numerical modelling, J. Mater. Res. Technol. 20 (2022) 2109–2172, https://doi.org/10.1016/j.jmrt.2022.07.121.

[2] J.P.M. Pragana, R.F.V. Sampaio, I.M.F. Bragança, C.M.A. Silva, P.A.F. Martins, Hybrid metal additive manufacturing: a state–of–the-art review, Adv. Ind. Manuf. Eng. 2 (2021) 100032, https://doi.org/10.1016/j.aime.2021.100032.

[3] K.A. Lorenz, J.B. Jones, D.I. Wimpenny, M.R. Jackson, A review of hybrid manufacturing, in: International Solid Freeform Fabrication Symposium, 53, 2015, pp. 96–108. https://hdl.handle.net/2152/89311.

[4] X. Luo, M.C. Frank, A layer thickness algorithm for additive/subtractive rapid pattern manufacturing, Rapid Prototyp. J. 16 (2010) 100–115, https://doi.org/10.1108/13552541011025825.

[5] G. Ambrogio, F. Gagliardi, M. Muzzupappa, L. Filice, Additive-incremental forming hybrid manufacturing technique to improve customised part performance, J. Manuf. Process. 37 (2019) 386–391, https://doi.org/10.1016/j.jmapro.2018.12.008.

[6] F. Meiners, J. Ihne, P. Jürgens, S. Hemes, M. Mathes, I. Sizova, M. Bambach, R. Hama-Saleh, A. Weisheit, New hybrid manufacturing routes combining forging and additive manufacturing to efficiently produce high performance components from Ti-6Al-4V, Procedia Manuf. 47 (2020) 261–267, https://doi.org/10.1016/j.promfg.2020.04.215.

[7] M. Merklein, R. Schulte, T. Papke, An innovative process combination of additive manufacturing and sheet bulk metal forming for manufacturing a functional hybrid part, J. Mater. Process. Technol. 291 (2021) 117032, https://doi.org/10.1016/j.jmatprotec.2020.117032.

[8] Y. Li, R. Rapthadu, Bending-additive-machining hybrid manufacturing of sheet metal structures, in: Proceedings of the ASME 2017 12th International Manufacturing Science and Engineering Conference, vol. 1, 2017, https://doi.org/10.1115/MSEC2017-3062. V001T02A021.

[9] T. Papke, P. Dubjella, L. Butzhammer, F. Huber, O. Petrunenko, D. Klose, M. Schmidt, M. Merklein, Influence of a bending operation on the bonding strength for hybrid parts made of Ti-6Al-4V, Procedia CIRP 74 (2018) 290–294, https://doi.org/10.1016/j.procir.2018.08.113.

[10] F. Huber, T. Papke, M. Kerkien, F. Tost, G. Geyer, M. Merklein, M. Schmidt, Customized exposure strategies for manufacturing hybrid parts by combining laser beam melting and sheet metal forming, J. Laser Appl. 31 (2019) 022318, https://doi.org/10.2351/1.5096115.

[11] S. Rosenthal, S. Platt, R. Hölker-Jäger, S. Gies, S. Kleszczynski, A.E. Tekkaya, G. Witt, Forming properties of additively manufactured monolithic Hastelloy X sheets, Mater. Sci. Eng., A 753 (2019) 300–316, https://doi.org/10.1016/j.msea.2019.03.035.

[12] S. Rosenthal, M. Hahn, A.E. Tekkaya, S. Platt, S. Kleszczynski, G. Witt, Speeding up additive manufacturing by means of forming for sheet components with core structures, Int. J. Precis. Eng Manuf. - Green Tech. 9 (2022) 1021–1034, https://doi.org/10.1007/s40684-021-00384-x.

[13] C. López, A. Elías-Zúñiga, I. Jiménez, O. Martínez-Romero, H.R. Siller, J.M. Diabb, Experimental determination of residual stresses generated by single point incremental forming of AlSi10Mg sheets produced using SLM additive manufacturing, Materials 11 (2018) 2542, https://doi.org/10.3390/ma11122542.

[14] ASTM E8/E8M, Standard Test Methods for Tension Testing of Metallic Materials, ASTM International, West Conshohocken, PA, USA, 2016. https://www.astm.org/e0008_e0008m-16.html.

[15] ASTM E290–14, Standard Test Methods for Bend Testing of Material for Ductility, ASTM International, West Conshohocken, PA, USA, 2022. https://www.astm.org/e0290-14.html.

[16] M.S.T. Sapage, J.P.M. Pragana, R.F.V. Sampaio, I.M.F. Bragança, C.M.A. Silva, P.A.F. Martins, Multi-planar injection lap riveting, J. Adv. Join Proc. 9 (2024) 100175, https://doi.org/10.1016/j.jajp.2023.100175.

[17] C.V. Nielsen, P.A.F. Martins, Finite element flow formulation, in: Metal Forming: Formability, Simulation and Tool Design, Academic Press, London, 2021, pp. 181–247, https://doi.org/10.1016/B978-0-323-85255-5.00008-X.

[18] K. Mattiasson, FE-models of the sheet metal forming processes, in: D. Banabic (Ed.), Sheet Metal Forming Processes: Constitutive Modelling and Numerical Simulation, Springer-Verlag, 2010, pp. 1–24, https://doi.org/10.1007/978-3-540-88113-1_1.

[19] L. Thijs, K. Kempen, J.P. Kruth, J. Van Humbeeck, Fine-structured aluminium products with controllable texture by selective laser melting of pre-alloyed AlSi10Mg powder, Acta Mater. 61 (2013) 1800–1819, https://doi.org/10.1016/j.actamat.2012.11.052.

[20] P.A.F. Martins, N. Bay, A.E. Tekkaya, A.G. Atkins, Characterization of fracture loci in metal forming, Int. J. Mech. Sci. 83 (2014) 112–123, https://doi.org/10.1016/j.ijmecsci.2014.04.003.

[21] F.A. McClintock, A criterion for ductile fracture by the growth of holes, J. Appl. Mech. 35 (1968) 363–371, https://doi.org/10.1115/1.3601204.